# A Computationally Efficient PM Power Loss Mapping for Brushless AC PM Machines with Surface-Mounted PM Rotor Construction

Xiaopeng Wu, Rafal Wrobel, *Senior Member*, *IEEE*, Phil H. Mellor, Chengning Zhang

***Abstract*** **-- This paper describes a computationally efficient approach for mapping the rotor power loss in permanent magnet (PM) machines. The PM loss mapping methodology discussed here utilises a small number of time-step finite element analyses (FEA) to determine the parameters of a functional representation of the loss variation with speed (frequency) and stator current, and is intended for a rapid evaluation of machine performance over entire torque-speed envelope. The research focus is placed on field-oriented controlled brushless AC PM machines with surface-mounted PM rotor construction, although the method could be adapted for other rotor formats. The loss mapping procedure accounts for the axial-segmentation of PM array through the use of an equivalent electrical resistivity of the segmented PM array, obtained from 3D FEA. The PM loss can be accurately mapped across the full operational envelope, including the field weakened mode, through a single three-dimensional (3D) and four two-dimensional (2D) time-step FEAs. The proposed methodology is validated on an 18 slots, 16 poles surface-mounted brushless AC PM machine design. The loss mapping procedure results agree closely with the computationally demanding alternative of direct 3D FE prediction of the PM power loss undertaken at each of the machine's operating points.**

***Index Terms*— PM power loss, surface-mounted brushless AC PM machines, computationally efficient methodology, loss mapping, finite element analysis (FEA), segmented PM array.**

## I. INTRODUCTION

THE accurate prediction of loss and its variation with load is an important element in the design of electrical machines [1]. Vehicle propulsion applications are particularly demanding as the understanding of machine efficiency over the entire working envelope and under specific control and operating conditions is usually required [2]-[4]. Typically an electric propulsion motor operates under constant torque and field-weakened control regimes. Further the motor input voltage at a given operating point can be highly variable, depending on the battery state of charge. The loss derivation, in such cases, is a time demanding and computationally intensive process requiring numerous analyses to predict each component of loss over the full range of operation.

In general, the sources of loss present within an electric machine can be categorised as mechanical and electromagnetic. Mechanical loss is attributed to the frictional effects within the bearing assembly (bearing loss) and fluid dynamics or aerodynamics effects within the motor body (windage or drag loss) [5]. Electromagnetic losses are usually associated with active parts of the motor assembly and include the iron, winding and permanent magnet (PM) loss components [6]-[8].

Recently, there has been increased interest in methods for accurate and computationally efficient derivation of the electromagnetic loss components [1], [9], [10], that can be easily incorporated within design software tools. Of particular interest is the automated generation of loss/efficiency maps, which have received some attention in the literature [1], [9]. Proposed techniques for the calculation of iron and winding loss components are based on functional representations of the analysed loss components, where the loss function parameters are informed from experiment and/or theoretical analyses. A common approach makes use of a limited number of finite element analyses (FEAs) to populate the loss function parameters, and allows for rapid and accurate loss derivation at multiple operating points across a machine's working envelope.

As permanent magnet material is widely used in electric machines, including, e.g., industrial machines, wind power generators, traction motors, high speed machinery, and machines used in aerospace applications [11]-[14], the power loss associated with the permanent magnet (PM) rotor assembly has been drawing more attention. This loss component is particularly important as excessive rotor temperature may result in premature failure. High rotor temperature will lead to a reduction in the torque and in some severe cases irreversible demagnetization of the PM array. Since heat is not easily dissipated from the rotating PM assembly either the magnet loss has to be kept at a manageable level or enhanced means of rotor cooling need to be introduced. This is exacerbated by difficulty of predicting rotor temperature; the rotary rotor assembly does not allow for a simple and reliable temperature monitoring and protection. Furthermore, the continuous drive towards high power-density and compact PM machine solutions imposes the requirement of elevated temperature operation to fully utilise physical properties of the active materials used.

Although there are both eddy-current loss component and hysteresis loss component occur in PMs [15], researchers always focus on eddy-current loss, with hysteresis ignored. When reviewing the existing techniques of predicting magnet loss in the rotors of PM machines, two main methods have emerged: numerical and analytical [10], [16]-[36]. The numerical approach includes time-stepping or frequency domain FEA and is commonly used to calculate the induced eddy currents in the magnets from which corresponding Joule losses are determined. Two-dimensional (2D) FEA is used predominantly in the analysis of radial-flux machines. For other less common machine topologies, e.g. axial-flux and transverse-flux, and laminated PM array constructions, three-dimensional (3D) FEA is usually required. The FE approach is time consuming and computationally intensive, in particular

Xiaopeng Wu and Chengning Zhang are with the School of Mechanical and Vehicular Engineering, Beijing Institute of Technology, Beijing, 10006, China. (e-mail: 3120100189@bit.edu.cn).

Rafal Wrobel and Phil H. Mellor are with the Department of The authors are with the Department of Electrical and Electronic Engineering, University of Bristol, Bristol, BS8 1UB, U.K.

when 3D analysis is needed. This makes the FE based approach difficult to be adopted within automated design approaches and in multi-physics or thermal analysis.

A variety of analytical techniques have been proposed for predicting magnet loss. These are based on simplified assumptions of the field distribution and their use is limited to the selected machine topologies for which the assumptions hold. In general each analytical method caters for a single loss mechanism. For example analytical techniques are available to account for the loss resulting from the stator slotting [19]-[25], whereas other methods deal with the armature reaction [26]-[40]. Hybrid techniques combine a simplified magneto-static FEA with analytical formulae for estimating the magnitude of the induced eddy current loss [10]. This approach benefits from both methods providing accurate PM loss prediction in a timely manner. However, a degree of proficiency in using FEA is required to fully benefit from the hybrid approach.

Segmentation of the PM array is a commonly adopted procedure for reducing magnet loss. Since segmentation adds significant cost it is important to obtain the correct balance between loss reduction and manufacturing complexity, and accurate loss prediction is key to this. Some of the existing analytical techniques include provision for circumferential and/or axial segmentation along with other effects such as eddy current reaction [41], [42]. The 3D nature of segmentation means such analytical formulations are complex and are not easy accessible to non-specialists.

In this paper a hybrid computationally efficient approach for mapping the rotor power loss in permanent magnet (PM) machines is proposed. The method uses a small number of FEAs to determine the parameters of a functional representation of the PM loss variation with speed (frequency) and stator current. The polynomial form of the loss function has been established based on initial series of exploratory FEAs [43]. This initial work has shown that the proposed approach provides an accurate mapping of PM loss across the full working envelope and is further developed here to cater for magnet segmentation. An equivalent electrical resistivity for the segmented PM array is introduced to cater for the increase in the eddy current paths. This equivalent electrical resistivity is found from a 3D FEA and, when substituted for the PM material resistivity, yields accurate results from a 2D FEA model. The loss predictions from 2D FE analyses are then used to define a functional representation of the PM loss analogous to that shown in [43]. The complete methodology is discussed in detail and demonstrated on a machine design exemplar showing close correlation with the direct FE PM loss predictions.

The remainder of the paper is organised in the following manner: Section II outlines the machine design exemplar together with FEA model definition; Section III describes the modified resistivity approach for an axially-segmented PM array; Section IV details the PM loss mapping approach and Section V summarizes the research findings.

## II. MACHINE EXEMPLAR

### A. Machine Design Exemplar

An external rotor fractional-slot machine design exemplar has been chosen to demonstrate the approach. An outline of the machine cross-section is shown in Fig. 1, and basic machine data is listed in Table I. This machine design exhibits excessive PM loss resulting largely from slotting effects attributed to the open-slot stator construction [43]. An open slot construction would allow the use of preformed coils leading to a low cost winding assembly with an excellent conductor fill factor [3]. In order to reduce the loss axial segmentation of the PM array has been considered, as such a construction is more common and cost effective [44].

A three phase, star connected, double-layer concentrated winding construction is used. The respective pole and slot number are $p = 16$ and $q = 18$. The design requires a base speed of 4000rpm and a maximum operating speed of 6000rpm; the ratio of maximum to base speed is therefore 1.5. The laminated core packs are made of SiFe (M300-35A), and the magnets are formed from a NdFeB grade with $B_r = 1.16$T and $H_c = 987$A/m.

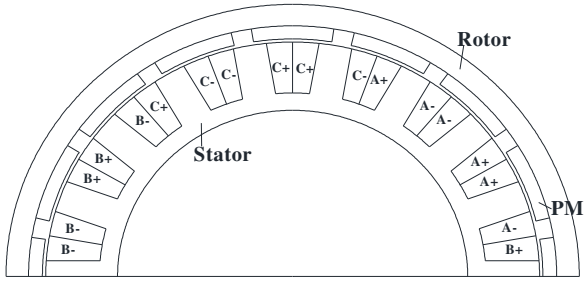


Fig. 1. Cross-section of the analysed PM motor design -2D FE model representation

TABLE I. MOTOR DESIGN DATA

| | |
|---|---|
| Number of poles | 16 |
| Number of slots | 18 |
| Number of phases | 3 |
| Rated speed | 4000rpm |
| Rated torque | 35Nm |
| Rated power | 14.7kW |
| Maximum speed | 6000rpm |
| Motor outer diameter | 175mm |
| Stator outer diameter | 150.8mm |
| Slot opening | 16.1mm |
| Slot depth | 16.4mm |
| Tooth width | 10.1mm |
| Active length | 55mm |
| Magnet thickness | 4.2mm |
| Air-gap thickness | 1mm |
| PM material | NdFeB |
| Electrical resistivity of PM | 1.8e-4 Ωcm |

### B. Electromagnetic Finite Element Model

The modelling technique employed here to derive the PM loss makes use of commercially available 2D and 3D time-step FE solvers [45]. To minimise computation time and following established practice, the FE model definition accounts for geometrical/topological symmetries present in the analysed motor design. The generated PM loss is determined from the Joule loss:

$$P = \iiint_V \boldsymbol{E} \cdot \boldsymbol{J} dV = \rho \iiint_V \boldsymbol{J}^2 dV = \rho l \iint_S J^2 dS \quad , \qquad (1)$$

where $l$ is the equivalent active length of the machine, $\rho$ is the electrical resistivity of PM material at working temperature $T$ and $J$ is the current density, $E$ is the density of PM electric field, $V$ is the volume of PM blocks and $S$ is the cross sectional area of PM in 2D FEA.

Due to periodic symmetry, circumferentially only a half of the complete motor cross-section is modelled, Figs. 1 and 2. Axial symmetry of the motor allows for the 3D FE model to be further reduced to one quarter of the overall machine volume. For the segmented PM array, a model depth of half of axial length of a single PM segment is adopted as shown in Fig 3. Whilst this model definition provides a computationally efficient solution it overlooks end effects. In the case of machine designs with relatively low aspect ratio of the active length to outer diameter, end-effects can have a prominent impact. Also, it is important to note that both the 2D and 3D FE solvers employed in the analysis account for the material magnetic nonlinearity.

Figs. 4 and 5 illustrate distribution of magnetic flux density within the stator and rotor core packs together with vector plot of the eddy-currents in the PM poles from 2D and 3D FEA at rated operation, $n$ = 4000rpm, $I_q$ =177A$_{rms}$. Here, the exemplar machine design is fitted with a non-segmented PM array.

An initial 3D FEA study has shown that effects due to the finite machine total active length and end-windings have a moderate impact on the PM loss predictions, Fig. 6. The half-segment 3D model errs to a ~10% overestimate of the magnet loss. The end-effects associated with the end-winding region are therefore not treated in this analysis.

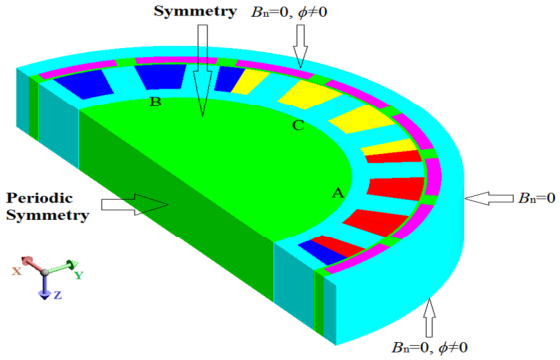


Fig. 2. 3D FE model of the analysed motor showing boundary conditions

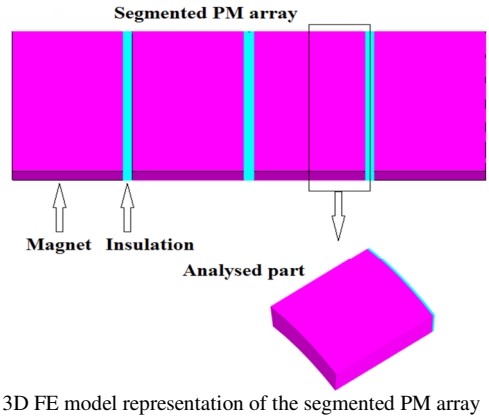


Fig. 3. 3D FE model representation of the segmented PM array

In general, the electrical resistivity of sintered rare-earth PM materials is anisotropic and varies with reference to the magnetisation axis of a PM material sample [46]. Here isotropic properties of the PM material has been assumed in the FE solver, see Table I. The temperature variation of the PM electrical resistivity is also an important factor. The results given in this paper are based on fixed PM temperature of 20°C. Since the electrical resistivity of the sintered rare-earth PM materials changes approximately linearly with temperature [46], it would be possible to incorporate this temperature variation through interpolation between two loss analyses data sets performed at different temperature set points. It is important to note that the FE power loss analysis at a given PM temperature assumes a uniform temperature distribution within the PM array. Due to localised nature of the PM loss and dissimilar heat transfer mechanisms from the rotor inner and outer surfaces that might not always to be the case. Thus the PM temperature used in the power loss analysis refers to an average over the PM array.

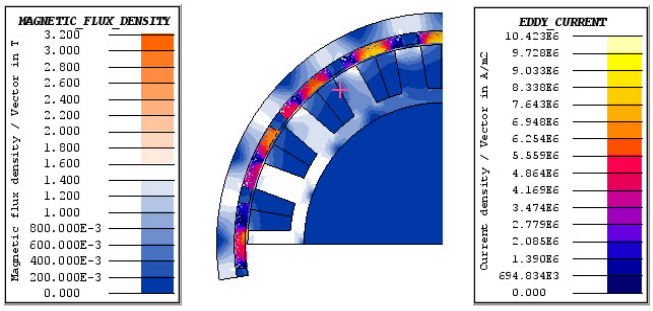


Fig. 4. Distribution of magnetic flux density within the stator and rotor core packs together with vector plot of the eddy-currents in the PM poles from 2D FEA – rated operation, $n$ = 4000rpm, $I_q$ =177A$_{rms}$

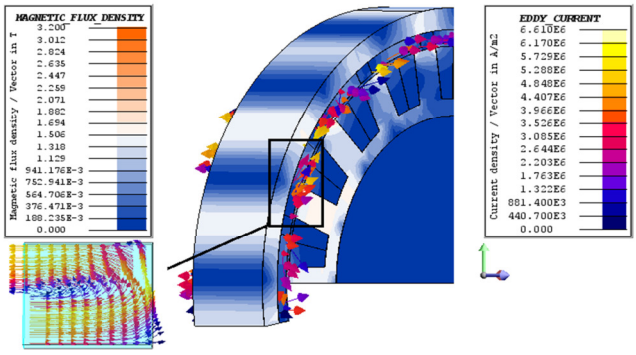


Fig. 5. Distribution of magnetic flux density within the stator and rotor core packs together with vector plot of the eddy-currents in the PM poles from 3D FEA – rated operation, $n$ = 4000rpm, $I_q$ =177A$_{rms}$, non-segmented PM array

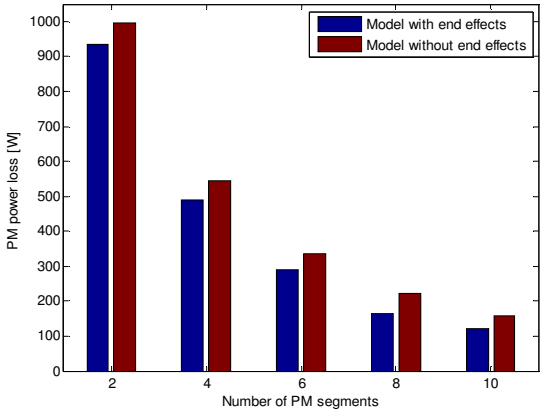


Fig. 6. PM power loss predictions vs. number of PM segments at open-circuit operation, $n$ = 4000rpm

## III. Incorporation of 3D Effects in PM Loss Model

In general, a 2D FE model representation of a radial-flux

machine assumes that the end-effects are insignificant and the machine's cross-section is accounted for only. Consequently the 2D model neglects the circumferential return path of the eddy-currents at the finite axial boundaries of the PM segments and as a result will overestimate the PM loss predictions. For example, Fig. 7 presents the FEA calculated PM loss during no-load (open circuit) operation for the exemplar machine design fitted with a non-segmented PM array. Here, the PM loss is attributed entirely to the loss component from the slotting effect. The results indicate a significant discrepancy between the 2D and 3D FEA loss calculations, the 2D analysis overestimating the loss by around a factor of 2.5. The results also indicate the PM loss would be prohibitively high in the open slot design considered without segmentation of the magnets.

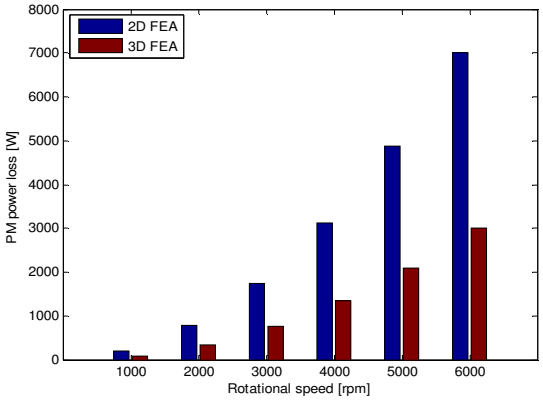


Fig. 7. PM power loss predictions versus rotational speed at open-circuit operation for non-segmented PM array

Analytical techniques allow for the additional length of the return path to be included in the PM loss derivation [10]. The alternative considered here is to adjust the value of the permanent magnet resistivity used in a 2D FEA model to compensate for the increased path length. Assuming the induced eddy currents are entirely resistance limited in the magnet regions, the resistivity correction factor will be equal to the ratio of the loss calculated by an uncorrected 2D solution compared to the full 3D model predictions:

$$\eta = \frac{P_{PM-2D}}{P_{PM-3D}} \; ; \; \rho_{2D} = \eta \rho_{PM} \quad , \qquad (2)$$

Where $P_{PM\text{-}2D}$ and $P_{PM\text{-}3D}$ are PM loss predictions from 2D and 3D FEA respectively, $\rho_{PM}$ is the PM material resistivity (1.8e-4Ω·cm for NdFeB at 20°C) and $\rho_{2D}$ is the equivalent resistivity used in the 2D FEA. The correction factor (2) is specific to a particular electromagnetic design; the machine geometry, the degree of segmentation, the choice of materials etc. However the same resistivity adjustment should apply to slotting induced losses and stator current induced losses. Consequently a single correction factor applies across the entire motor operating regime; in the example design $\eta = 2.3$ for a rotor with no axial segmentation. Similarly it would be expected the variation of loss with magnet temperature could be addressed by scaling (2) by the applicable temperature coefficient of resistivity.

In machine designs where slotting induced eddy current losses are significant, such as the open slot design considered here, the open-circuit PM loss calculations can be used to find the correction factor. In these circumstances (3) applies.

$$\eta = \frac{P_{PM-SE-3D}}{P_{PM-SE-2D}} \quad , \qquad (3)$$

where $P_{PM\text{-}SE}$ is the PM loss component from the slotting effect derived at open-circuit operation of the analysed machine.

Fig. 8 compares the PM loss predictions at three arbitrary operating points, calculated using 2D FEA, 2D FEA with the correction (3) applied and 3D FEA. The results are for a non-segmented rotor design during open circuit, field weakened and maximum torque per amp operation. The $I_d$, $I_q$ nomenclature given in Fig. 8 refers to the $dq0$ machine model representation [47]. The results confirm that the proposed correction provides a close correlation to the loss derived from full 3D FEA across a range of operation conditions. The PM loss mapping methodology described later in this paper aims to provide a computationally efficient and simple to implement algorithm based upon a minimal number of FEA solutions. The use of 3D FEA is confined to determining the eddy current path correction factor (2), which is then incorporated in all subsequent 2D FEA.

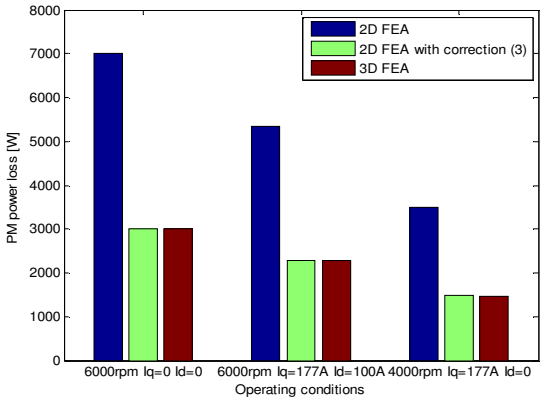


Fig. 8. PM power loss predictions at a number operating points employing various FE based PM loss derivation techniques

The approach is equally applicable to multiple magnet segmentations. Again a single resistivity compensation factor can be found by comparing the loss predictions from 3D FEA for the segmented rotor design to the uncompensated 2D FEA results:

$$\rho(u) = \eta(u)\rho_{PM}; \; \eta(u) = \frac{P_{PM-SE-3D}(u)|_{\rho_{PM}}}{P_{PM-SE-2D}|_{\rho_{PM}}} \quad , \qquad (4)$$

where $\rho(u)$ is the compensated electrical resistivity of a segmented PM array, the index $u$ denotes the number of PM segments $\rho_{PM}$ is the inherent electrical resistivity of the PM material, $P_{PM-SE-2D}|_{\rho_{PM}}$ is the 2D FEA loss prediction calculated using the uncompensated value of magnet resistivity $\rho_{PM}$, whereas $P_{PM-SE-3D}(u)|_{\rho_{PM}}$ is the 3D FEA loss prediction for the PM array with $u$ segments. Note the FEA should be executed for the same operating conditions.

The validity of the proposed method is confirmed in Fig. 9 where the PM loss predictions directly from 3D FEA are

compared to the 2D FEA calculations with the compensated resistivity (4). Here the PM loss during open-circuit operation is considered with increasing number $u$ of axial segments. A simplified 2D FEA using a corrected equivalent electrical resistivity can be used to provide an accurate estimation of loss in a segmented PM array. Fig. 10 presents the value of compensated resistivity used in the 2D FEA applicable to the example machine. As would be expected, the equivalent electrical resistivity of the PM material $\rho(u)$ increases with the number of PM segments. It is important to note that employing 8 axial PM segments per pole would reduce the PM loss by 80%.

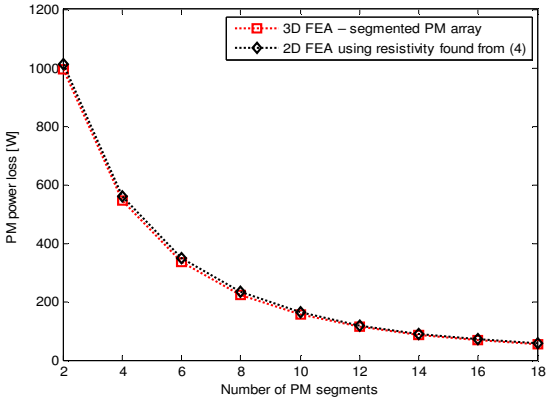


Fig. 9. Calculated PM power loss versus number of PM segments at open-circuit operation, $n$ = 4000rpm – illustration of the equivalent electrical resistivity approach for the segmented PM array

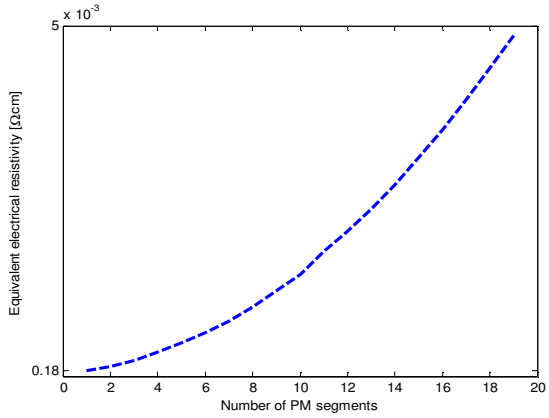


Fig. 10. The equivalent electrical resistivity of the PM material $\rho(u)$ versus number of PM segments

## IV. PM Power Loss Mapping

The eddy current loss generated in the PM array stems from two effects. The first results from the permeance variation caused by stator slotting, $P_{PM\text{-}SE}$, and the second from the armature reaction field, $P_{PM\text{-}AR}$, [19]-[36], [43].

The armature reaction loss is a consequence of the higher order spatial harmonics of the winding distribution, and, in the case of non-sinusoidal phase currents, temporal harmonics. This loss component strongly depends on the control scheme and operating mode of an electrical machine. Here the phase current is assumed to be sinusoidal with any current control or high-frequency PWM effects neglected.

The following function provides an accurate map of the magnet loss over the entire torque-speed envelope [43]:

$$P_{PM} = \left(aI_q^2 + bI_d^2 + cI_d + d\right)\left(\frac{n}{n_W}\right)^2 \quad , \qquad (5)$$

where $I_q$ is the quadrature-axis current, $I_d$ is the direct-axis current and $n$ is the rotational speed. The coefficients $a$, $b$, $c$, $d$ are evaluated through four individual time-stepping FEAs undertaken at a reference speed $n_W$.

In general, the armature reaction has an effect on the PM loss component from the stator slotting, $P_{PM\text{-}SE}$. This results from the $d$-axis excitation, $I_d$, which increases or decreases the $d$-axis flux depending on machine's operating regime. The first two components on the right hand side in (5), $aI_q^2$ and $bI_d^2$, are attributed with the PM loss from armature reaction harmonics, $P_{PM\text{-}AR}$, whereas the last two terms, $cI_d$ and $d$, account for the PM loss associated with the stator slotting harmonics, $P_{PM\text{-}SE}$. In particular, $cI_d$ accounts for $I_d$ effect on the $P_{PM\text{-}SE}$. It is important to note that the proposed approach treats the armature reaction and slotting harmonics in a decoupled manner. Consequently for the machine designs where interaction between these two effects is insignificant, the proposed approach provides good correlation with the direct PM loss predictions from FEAs. For machine designs, where these effects are more prominent, the PM loss mapping will yield reduced accuracy.

Moreover, when the reaction field from the PM rotor is significant, e.g. for a non-segmented PM array with prohibitively high power loss, the proposed method will exhibit lesser accuracy. In addition to that, for the machine designs, where the PM loss is inductance-limited, i.e. significant skin effect in the PM array, the coefficients $a$, $b$, $c$ and $d$ in (5) would need to be adjusted with the operating load conditions. The proposed PM mapping approach in its current form is not applicable for the cases, where the PM loss is inductance-limited. However, as the segmented PM array arrangement is commonly used in construction of electrical machines to reduce the PM loss, it is expected that in the majority cases the PM loss will be resistance-limited. This results from relatively small geometrical dimensions of PM segments per rotor poles in respect to the skin depth.

Furthermore, magnetic saturation of the stator and rotor core materials has an effect on accuracy of the PM loss mapping technique as it has been shown in [43]. At elevated excitation, the magnetic saturation 'softens' the severity of change of the magnetic flux seen by the PM array and consequently results in reduced PM loss. It is possible to include the magnetic saturation effect in (5), but this would require additional FEAs to define the form of the saturation relationship. It is important to note that in the analysis both the rotor and stator core packs are laminated.

### A. *Inclusion of Magnet End Effects and Segmentation*

To incorporate end effects and segmentation of the magnet array in loss predictions it is possible to generate parameters for (5) directly from 3D FEAs. However a loss mapping process based entirely on 3D FEAs would be computationally demanding. The 2D FEA with a compensated PM resistivity approach described in the previous section would significantly reduce this computation overhead. In the machine example the open-circuit losses are significant and this can be used to determine resistivity correction factor:

$$\eta(u) = \frac{P_{PM-SE-3D}\,(u)|_{n_W,\rho_{PM}}}{P_{PM-SE-2D}|_{n_W,\rho_{PM}}} \quad , \qquad (6)$$

where $P_{PM-SE-2D}|_{n_W,\rho_{PM}}$ is the 2D FE open-circuit PM loss prediction using electrical resistivity $\rho_{PM}$ at speed $n_W$.

For motor designs with an axially segmented PM array with $u$ segments per PM pole, the magnet loss function for the entire torque-speed envelope given by (5) can be rewritten as:

$$P_{PM} = \begin{pmatrix} a|_{\rho(u)} I_q^2 + b|_{\rho(u)} I_d^2 \\ +c|_{\rho(u)} I_d + d|_{\rho(u)} \end{pmatrix} \left(\frac{n}{n_W}\right)^2 \quad . \qquad (7)$$

Here, the subscript $\rho(u)$ indicates that the related coefficients are calculated using 2D FEA with an equivalent PM electrical resistivity found using (6).

### *B. Maximum Torque per Ampere Operation*

In the constant torque operation region, the motor is usually controlled at rated flux to minimise the current for a given torque. With the non-salient rotor designs this operation corresponds to the phase current ($I_{ph}$) being aligned to the quadrature-axis, i.e. $I_d = 0$, $I_q = I_{ph}$, therefore (7) can be written in a simplified form:

$$P_{PM} = \left(a|_{\rho(u)} I_q^2 + d|_{\rho(u)}\right) \left(\frac{n}{n_W}\right)^2 \quad , \qquad (8)$$

To inform the functional representation of PM loss (8), parameter $d$ refers to the previously described 2D FEA at open-circuit operation (with the accompanying 3D FEA to determine the PM resistivity correction). A supplementary 2D FEA is required to find parameter $a$, which evaluates the PM loss at rated current with $I_q = I_{ph}$ and at the same rotational speed as for the open-circuit analysis. From the 2D FEA, the armature reaction PM loss component can be obtained by subtracting the PM loss at the open-circuit operation from the total PM loss at the rated, maximum torque per Ampere operation. The coefficients $d$ and $a$ are thus determined as follows:

$$d = P_{PM-SE}|_{n_W} = P_{PM-SE-2D}|_{n_W,\rho(u)} \quad , \qquad (9)$$

and

$$a = \frac{P_{PM-AR-2D}|_{n_W, I_{qR}}}{I_{qR}^2} = \frac{P_{PM-2D}|_{n_W,\rho(u),I_{qR}} - P_{PM-SE-2D}|_{n_W,\rho(u)}}{I_{qR}^2} \quad , \qquad (10)$$

where $P_{PM-2D}|_{n_W,\rho(u),I_{qR}}$ is the 2D FE PM loss prediction using the corrected value of PM resistivity at the rated current $I_{qR}$ and rotational speed $n_W$. Consequently (8) is fully defined from three FEA solutions; 2D FEA for open circuit and rated current operation, and an open-circuit 3D FEA to determine the PM resistivity correction.

The accuracy of the PM mapping methodology is illustrated in Fig. 11. Two different levels of rotor segmentation for the analysed machine exemplar are considered; in the first the magnet array has 7 axial segments per pole, and in the second 19 axial segments per pole. Table II list the parameters used in the analysis. The parameters have been obtained from open-circuit and rated excitation at $I_{qR}$ = 177A$_{rms}$ FEAs at the same rotational speed $n_W$ = 5000rpm.

TABLE II. PARAMETERS OF THE MAGNET LOSS FUNCTION (8) FOR 7 AND 19 SEGMENTS.

| Number of segments | Parameter | | |
|---|---|---|---|
| | $\rho(u)$ [Ωcm] | $a$ [W/A$^2$] | $d$ [W] |
| 7 | 2.24e-3 | 6.9e-3 | 1150 |
| 19 | 1.28e-2 | 1.2e-3 | 204 |

Fig. 11 presents the PM loss obtained from 3D FEAs calculated for a range of quadrature axis currents $I_q$ and rotational speeds $n$. This data is compared against the PM loss predictions from the functional relationship (8) which are seen to correlate well with the directly derived FE results for two rotor segmentations considered. Over the range considered the error introduced by the simplified functional relationship is no more than 3%. This small discrepancy is attributed to the simplifying assumptions made regarding the PM resistivity correction used in the 2D FEA. In particular, the 2D FEA approach neglects any load dependent loss resulting from saturation of the machine's magnetic circuit.

### *C. Field Weakening Operation*

This section considers the form of the PM loss in the constant power, field weakened region of the torque-speed envelope commonly used in traction applications [3], [4]. At high speeds the resultant stator magnetic flux is weakened by injecting a direct-axis current component $I_d$, to create afield which opposes the PM excitation. This results in stator current containing both torque producing (quadrature axis) current and a field controlling (direct axis current), $I_{ph}(I_q, I_d)$, $I_d \neq 0$.

TABLE III. COEFFICIENTS $b$ AND $c$ FOR 7 AND 19 AXIAL SEGMENTS

| Number of Segments | Parameter | |
|---|---|---|
| | $b$ [W/A$^2$] | $c$ [W/A] |
| 7 | 9.4e-3 | -5.12 |
| 19 | 1.6e-3 | -0.89 |

a)

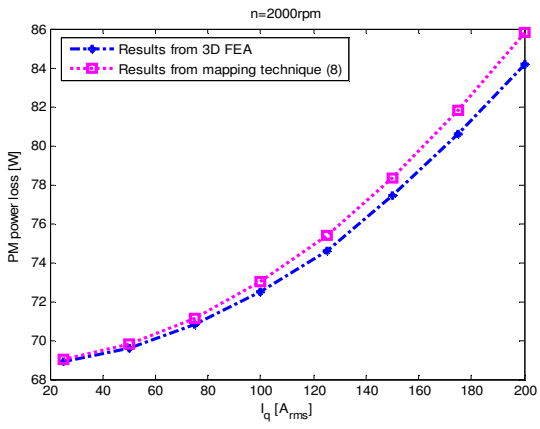


b)

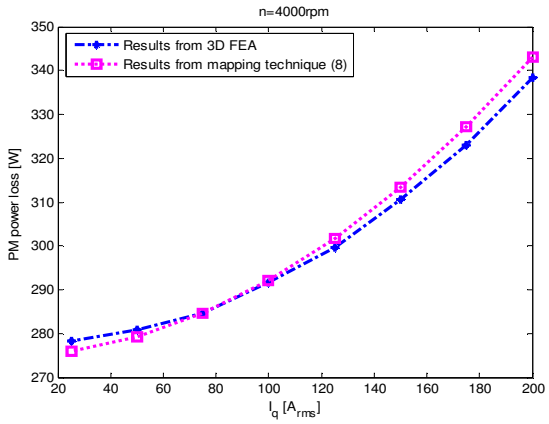


c)

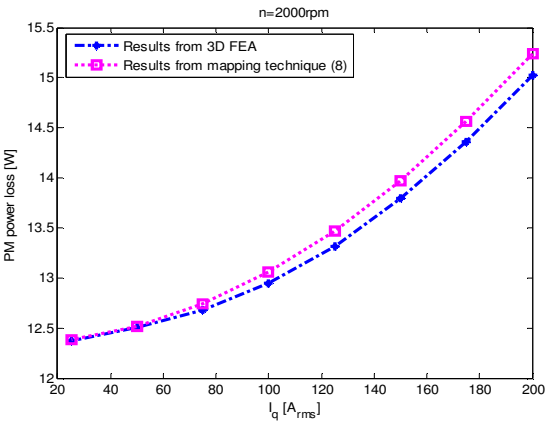


d)

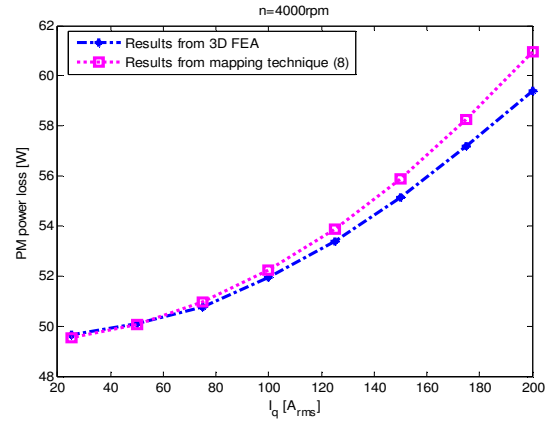


Fig. 11. PM power loss versus excitation current $I_{ph} = I_q$ and rotational speed for maximum torque per Ampere operation, a), b) 7 segment PM array $n$ = 2000rpm, $n$ = 4000rpm, c), d) 19 segment PM array, $n$ = 2000rpm, $n$ = 4000rpm

Fig. 12 illustrates the effectiveness of the proposed PM loss mapping procedure during field weakened operation. The PM loss obtained using the functional relationship (7) with the parameters given in Tables II and III are compared to the PM loss found from individual 3D FEAs evaluated at various operating points in the constant power region. For brevity results are only presented for a PM array with 7 axial segments, however similar agreement was obtained for the case of 19 axial segments. A maximum discrepancy of no more than 6% is observed across the operating range. Fig. 12 indicates that an increase in the field weakening $d$-axis current results in reduced PM loss.

Fig. 13 shows PM loss predictions at selected load points for the machine's field-strengthened operation to demonstrate deficiency of the PM mapping approach in accounting for the magnetic saturation. Note that the field-strengthened operation does not have any practical use in context of the analysed machine design and has been provided here for illustration purpose only. The results confirm that higher magnetic saturation of the machine's core material leads to larger discrepancies between the FE directly predicted and mapped PM loss data. Similar findings have been made in the authors' previous work [45], where alternative machine designs/topologies were analysed. The negative $I_d$ current listed in Fig. 13 indicates the field-strengthen operation as opposite to the field-weakened operation.

a)

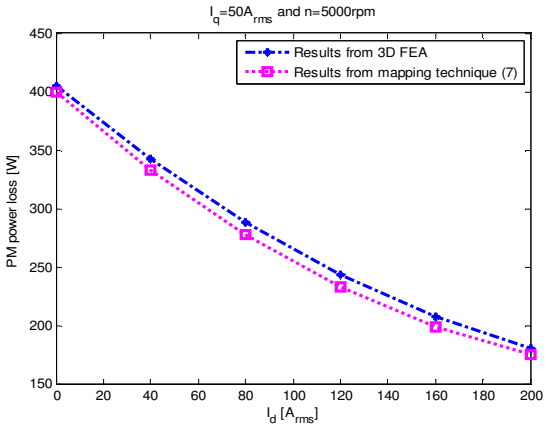


b)

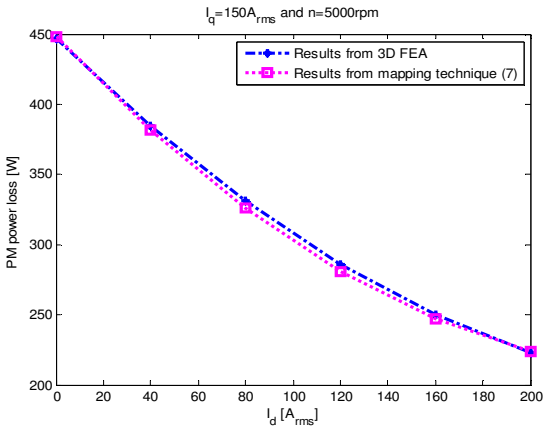


Fig. 12. PM power loss vs. $I_d$ current, a) $I_q$ = 50$A_{rms}$, $n$ = 5000rpm, b) $I_q$ = 150$A_{rms}$, $n$ = 5000rpm - 7 segment PM array

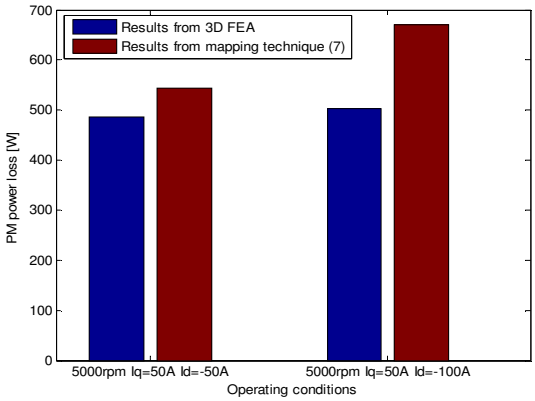


Fig. 13. PM power loss predictions at a number operating points for field strengthened operation – PM array with 7 segments per pole

### *D. Evaluation of loss mapping over entire torque-speed envelope*

The proposed functional relationship (7) enables the PM loss to be easily computed over an entire torque speed envelope. Fig. 15 compares the PM loss calculated directly from 3D FEAs with the proposed mapping approach over an illustrative torque-speed envelope, Fig. 14. Below 4000rpm maximum torque per Ampere control is enacted, between 4000rpm to 6000rpm the machine is field weakened. Here, an additional circumferential 4 and axial 7 segments PM array, together with mentioned axial 7 and 19 axial segments PM array are considered. For axial segments, the results clearly demonstrate the efficacy of the proposed PM loss mapping technique, while for circumferential segments, a small level of discrepancy can be found. This is attributed to the simplifying assumptions made regarding the PM resistivity correction used in the 2D FEA.

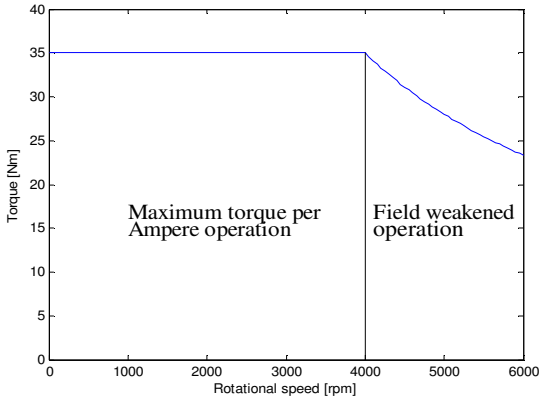


Fig. 14. Assumed rated torque-speed envelope of machine exemplar

a)

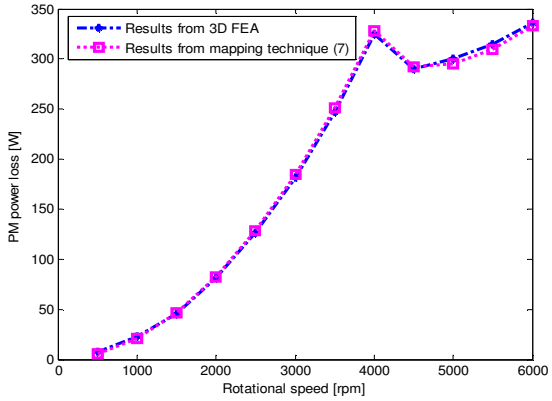


b)

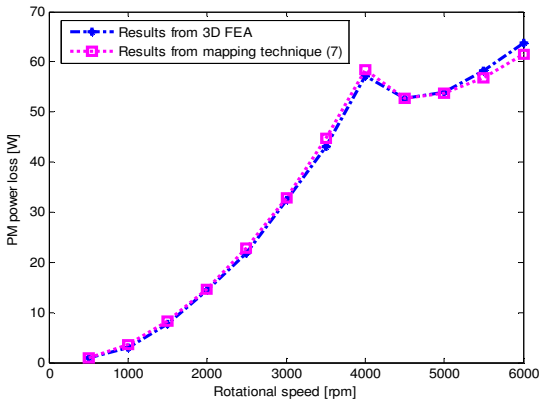


c)

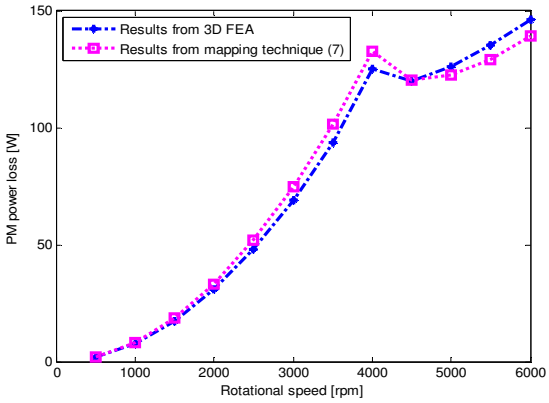


Fig. 15. Estimated magnet loss over the torque-speed envelope a) axial 7 segments PM array, b) axial 19 segments PM array, c) circumferential 4 and axial 7 segments PM array

## V. Summary of PM Loss Mapping Procedure

This section briefly summarises the procedure for obtaining the four parameters, $a$ to $d$, of the PM loss function (7) for a given rotor magnet array design $u$.

i. The PM loss component from the slotting effect is calculated using 3D FEA for open-circuit operation at a reference speed $n_W$

ii. A 2D FEA is also undertaken for open-circuit operation at the reference speed $n_W$, and at a nominal value of PM resistivity $\rho_{PM}$. The resistivity correction factor $\eta(u)$ (6) and the coefficient $d$ are then derived:

$$P_{PM-SE-3D}(u)|_{n_W}, P_{PM-SE-2D}|_{n_W,\rho_{PM}} \rightarrow \eta(u), \rho(u)$$

and using the corrected PM resistivity:

$$P_{PM-SE}|_{n_W,\rho(u)} \rightarrow d,$$

iii. The PM loss at the reference speed $n_W$ and rated excitation current for maximum torque per Ampere operation $I_{qR}$ is calculated from 2D FEA with the corrected PM resistivity. Parameter $a$ is found using:

$$a = \frac{P_{PM-2D}|_{n_W,\rho(u),I_{qR}} - P_{PM-SE-2D}|_{n_W,\rho(u)}}{I_{qR}^2}.$$

iv. The PM loss for two working points with $I_d$ current only, ($I_{d1W}$) and ($I_{d2W}$), and reference speed $n_W$ are calculated using 2D FEA with corrected PM resistivity. Coefficients $b$ and $c$ are then derived:

$$b = \frac{P_{PM-AR-2D}|_{n_W,I_{d1W},\rho(u)} \cdot I_{d2W} - P_{PM-AR-2D}|_{n_W,I_{d2W},\rho(u)} \cdot I_{d1W}}{I_{d1W}^2 \cdot I_{d2W} - I_{d2W}^2 \cdot I_{d1W}}$$

$$c = \frac{P_{PM-AR-2D}|_{n_W,I_{d1W},\rho(u)} \cdot I_{d2W}^2 - P_{PM-AR-2D}|_{n_W,I_{d2W},\rho(u)} \cdot I_{d1W}^2}{I_{d2W}^2 \cdot I_{d1W} - I_{d1W}^2 \cdot I_{d2W}}.$$

In the example presented in the paper $I_{d1W}$ is set to be equal to 10% of rated current, and $I_{d2W}$ is set to the rated current. The reference speed $n_W$ at which the loss coefficients are evaluated should be set within the field weakened regime of the torque-speed envelope. If field weakened operation is not required steps iv) can be omitted. Depending on a particular application and operating points

of interests excitation with injected direct axis current may not be of concern and the simplified version of the magnet loss scaling function according to (8) might be more applicable.

## VI. CONCLUSIONS

A simple and computationally efficient methodology for estimating magnet eddy current losses across the full operational envelope of a brushless PM AC machine has been presented. The approach outlined in this paper builds on the authors' previous work on PM loss mapping, to include an accurate representation of end effects and magnet segmentation. An equivalent electrical resistivity for the PM array has been introduced to maintain the computational efficiency of the original approach, which was based upon undertaking a small number of 2D FEA to determine the parameters of a functional relationship describing the loss. A single further 3D FEA is required to establish this equivalent electrical resistivity for the particular segmented PM array to be analysed. The proposed approach caters for both slotting and armature reaction loss effects. Although confined to sinusoidal excitation only, it provides a valuable addition to the evaluation of loss and thermal performance for the entire torque-speed envelope.

In total only four individual 2D time-stepping FEAs and a single 3D FEA are required to fully inform the parameters of the function describing the PM loss. The 2D FEA comprise: open-circuit operation, rated current with $I_q$ only operation, rated current and 10% of rated current with $I_d$ only operation, all at the same reference rotational speed. Provided the PM loss due to slotting effects is significant the 3D FEA is limited to open-circuit operation only. This allows for a simplified and less time consuming model definition, where the winding assembly is not accounted for in the model. Consequently the computational overhead associated with the method is small.

The proposed methodology has been compared against the results from individual 3D FEA at every operating point, showing close correlation across the full working envelope. A number of examples illustrating the use and fidelity of the proposed technique have been given. These include rotor construction with differing levels of segmentations for the analysed machine exemplar.

## VII. REFERENCES


[1] P.H. Mellor, R. Wrobel, D. Holiday, "A Computationally Efficient Iron Loss model for Brushless AC Machines that Caters for Rated Flux and Field Weakened Operation," *IEEE International Conference on Electrical Machine and Drives,* 2009, IEMDC'09, pp. 490-494.

[2] J. Goss, R. Wrobel, P.H. Mellor, D. Staton, "The Design of AC Permanent Magnet Motors for Electric Vehicles: A Design Methodology," *IEEE International Conference on Electric Machines and Drives,* 2013, IEMDC'13, pp. 871 – 878.

[3] R. Wrobel, J. Goss, A. Mlot, P.H. Mellor, "Design Considerations of a Brushless Open-Slot Radial-Flux PM Hub Motor," *IEEE Trans. Ind. Appl*., vol. 50, no. 3, pp. 1757-1767, 2014.

[4] J. Goss, P.H. Mellor, R. Wrobel, D.A. Staton, M. Popescu, "The Design of AC Permanent Magnet Motors for Electric Vehicles: A Computationally Efficient Model of the Operational Envelope," *6th IET International Conference on Power Electronics, Machines and Drives,* 2012, PEMD'12, pp. 1– 6, 2012.

[5] R. Wrobel, G. Vainel, C. Copeland, T. Duda, D. Staton, P.H. Mellor, "Investigation of Mechanical Loss and Heat Transfer in An Axial-flux PM Machine," *Energy Conversion Congress and Exposition,* 2013, ECCE'13, PP. 4372 – 4379.

[6] D. A. Howey, A. S. Holmes, K. R. Pullen, "Measurement and CFD Prediction of Heat Transfer in Air-Cooled Disc-Type Electrcal Machines," *IEEE Trans. Ind. Appl.,* vol. 47, no. 4, pp. 1716 – 1723, 2011.

[7] D. A. Howey, A. S. Holmes, K. R. Pullen, "Measurement of Stator Heat Transfer in Air-Cooled Axial Flux Permanent Magnet Machines," *35th IEEE Industrial Electronics Annual Conference*, 2009, IECON'09, pp. 1197 – 1202.

[8] A. C. Malloy, R. F. Martinez-Botas, M. Jaensch, M. Lamperth, "Measurement of Heat Generation Rate in Permanent Magnet Rotating Electrical Machines," *6th IET International Conference on Power Electronics, Machines and Drives,* 2012, PEMD'12, pp. 1– 6, 2012.

[9] R. Wrobel, D.E. Salt, A. Giffo, P.H. Mellor, "Derivation and Scaling of AC Copper Loss in Thermal Modeling of Electrical Machines," *IEEE Trans. Ind. Electron.,* vol. 61, no. 8, pp. 4412 – 4420, 2014.

[10] P. Zhang, G.Y. Sizov, J. He, D.M. Ionel, N.A.O. Demerdash, "Calculation of Magnet Losses in Concentrated-Winding Permanent-Magnet Synchronous MachinesUsing a Computationally Efficient Finite-Element Method," *IEEE Trans. Ind. Appl*., vol. 49, no. 6, pp. 2524 - 2532 , 2013.

[11] J. Nerg, M. Rilla, V. Ruuskanen, J. Pyrhönen, and S. Ruotsalainen, "Direct-driven interior magnet permanent magnet synchronous motors for a full electric sports car," *IEEE Trans. Ind. Electron.*, vol. 61, no. 8, pp. 4286–4294, Aug. 2014.

[12] P. Lindh, J. Montonen, P. Immonen, J. A. Tapia, and J. Pyrhönen, "Design of a traction motor with tooth-coil windings and embedded magnets," *IEEE Trans. Ind. Electron.*, vol. 61, no. 8, pp. 4306–4314, Aug. 2014.

[13] T. Baumgartner, R. M. Burkart, and J. W. Kolar, "Analysis and design of a 300-W 500 000-r/min slotless self-bearing permanent-magnet motor," *IEEE Trans. Ind. Electron.*, vol. 61, no. 8, pp. 4326–4336, Aug. 2014.

[14] T. D. Kefalas and A. G. Kladas, "Thermal investigation of permanent magnet synchronous motor for aerospace applications," *IEEE Trans. Ind. Electron.*, vol. 61, no. 8, pp. 4404–4411, Aug. 2014.

[15] J. Pyrhonen, S. Ruoho, J. Nerg, M. Paju, S. Tuominen, H. Kankaanpaa, R. Stern, A. Boglietti and N. Uzhegov, "Hysteresis Losses in Sintered NdFeB Permanent Magnets in Rotating Electrical Machines," *IEEE Trans. Ind. Electron.*, vol. 62, no. 2, pp. 857–865, Feb. 2015.

[16] X. F. Ding and C. Mi, "Modeling of Eddy Current Loss in the Magnets of Permanent Magnet Machines for Hybrid and Electric Vehicle Traction Application," *Vehicle Power and Propulsion Conference*, 2009, pp. 419-424.

[17] K. Yoshida, Y. Hita, K. Kesamaru, "Eddy-Current Loss Analysis in PM of Surface-mounted-PMSM for Electric Vehicles," *IEEE Trans. Magn.,* vol. 36, no. 4, pp. 1941-1944, 2000.

[18] M. Nakano, H. Kometani, M. Kawamura, "A Study on Eddy-Current Losses in Rotors of Surface Permanent Magnet Synchronous Machines," *IEEE Trans. Ind. Appl.,* vol. 42, no. 2, pp. 429-435, 2006.

[19] L. J. Wu, Z. Q. Zhu, D. Staton, M. Popescu, and D. Hawkins, "Analytical Modelling and Analysis of Open-circuit PM Power Loss in Surface-mounted Permanent Magnet Machines," *IEEE Trans. Magn.,* vol. 48, no. 3, pp. 1234-1246, 2011.

[20] Z. X. Fang, Z. Q. Zhu, L. J. Wu, Z. P. Xia, "Simple and Accurate Analytical Estimation of Slotting Effect on PM Power Loss in Fractional-Slot Surface-Mounted PM Machines," *IEEE International Conference on Electric Machine*, 2012, ICEM'12, pp. 464-470.

[21] D. A. Wills and M. J. Kamper, "Analytical Prediction of Rotor Eddy Current Loss due to Stator Slotting in PM Machines," *Energy Conversion Congress and Exposition*, 2010, ECCE'10, pp. 992-995.

[22] M. Markovic and Y. Perriard, "A Simplified Determination of the Permanent Magnet (PM) Eddy Current Losses due to Slotting in A PM Rotating Motor," *IEEE International Conference on Electrical Machines and Systems*, 2008, ICEMS'08, pp. 309-313.

[23] J. Alexandrova and H. Jussila, "Comparison between Models for Eddy-current Loss Calculations in Rotor Surface-mounted Permanent Magnets," *IEEE International Conference on Electrical Machines,* 2010, ICEM'10, pp. 978-982.

[24] S. M. Sharkh, A. Ali Qazalbash, N. T. Irenji, R. G. Wills. "Effect of Slot Configuration and Air-gap and Magnet Thicknesses on Rotor Electromagnetic Lloss in Surface PM Synchronous Machines," *IEEE International Conference on Electric Machine and Systems*, 2011, ICEMS'11, pp. 1-6.

[25] F. Caricchi, F. Giulii, F. Crescimbini and L. Solero Capponi, "Experimental Study on Reducing Cogging Torque and Core Power Loss in Axial-Flux Permanent-Magnet Machines with Slotted

Winding," *37th IEEE Annual Industry Applications Conference,* 2002, vol. 2, pp. 1295-1302.
[26] N. Schofield, K. Ng, Z. Q. Zhu, and D. Howe, "Parasitic Rotor Losses in A Brushless Permanent Magnet Traction Machine," *IEEE International conference on Electrical Machine and Drives,* 1997, IEMDC'97, pp. 200-204.
[27] H. Polinder and M. J. Hoeijmakers, "Eddy-current Losses in the Permanent Magnets of A PM Machine," *IEEE International Conference on Electrical Machines and Drives,* 1997, ICEM'97, pp. 138-142.
[28] H. Polinder and M. J. Hoeijmakers, "Eddy-current Losses in the Segmented Surface-mounted Magnets of A PM Machine," *IEE Proc-Electric Power Appl*., vol. 146, no. 3, pp. 261-266, 1999.
[29] Z. Q. Zhu, K. Ng, N. Schofield, and D. Howe, "Analytical Prediction of Rotor Eddy Current Loss in Brushless Machines Equipped with Surface-mounted Permanent Magnets. I. Magnetostatic field model," *IEEE International Conference on Electrical Machines and System*, 2001, ICEMS'01, pp. 806-809.
[30] N. Schofield, K. Ng, Z. Q. Zhu, and D. Howe, "Parasitic Rotor Losses in A Brushless Permanent Magnet Traction Machine," *IEEE International Conference on Electrical Machines and Drives*, 1997, IEMDC'97, pp. 200-204.
[31] K. Atallah, D. Howe, P. H. Mellor, and D. A. Stone, "Rotor Loss in Permanent-magnet Brushless AC Machines," *IEEE Trans. Ind. Appl*., vol. 36, no. 6, pp. 1612-1618, 2000.
[32] D. Ishak, Z. Q. Zhu, and D. Howe, "Eddy-current Loss in the Rotor Magnets of Permanent-magnet Brushless Machines having a Fractional Number of Slots per Pole," *IEEE Trans. Magn*., vol. 41, no. 9, pp. 2462-2469, 2005.
[33] J. Wang, K. Atallah, R. Chin, W. M. Arshad, and H. Lendenmann, "Rotor Eddy Current Loss in Permanent Magnet Brushless AC Machines," *IEEE Trans. Magn.,* vol. 46, no. 7, pp. 2701-2707, 2010.
[34] K. Yanazaki and A. Abe, "Loss Investigation of Interior Permanent Magnet Motors Considering Carrier Harmonics and Magnet Eddy Currents," *IEEE Trans. Ind, Appl*., vol. 45, no. 2, pp. 659-665, 2009.
[35] N. Bianchi and S. Bolognani, "An Overview of Rotor Losses Determination in the Three-phase Fractional-slot PM Machines," *IEEE Trans. Ind, Appl*., vol. 42, no. 2, pp. 429-435, 2010.
[36] W. Y. Huang, A. Bettayeb, R, Kaczmarek, and J. C. Vannier, "Optimization of Magnet Segmentation for Reduction of Eddy-Current Losses in Permanent Synchronous Machine," *Trans. Energy Convers.,* vol. 25, no. 2, pp. 381-387, 2010.
[37] M. Mirzaei, A. Binder and C. Deak, "3D Analysis of Circumferential and Axial Segmentation Effect on Magnet Eddy Current Losses in Permanent Magnet Synchronous Machines with Concentrated Windings," *IEEE International Conference on Electric Machine*, 2010, ICEM'10, pp. 1-6.
[38] M. Mirzaei, A. Binder, B. Funieru and M. Susic, "Analytical Calculations of Induced Eddy Currents Losses in the Magnets of Surface Mounted PM Machine with Consideration of Circumferential and Axial Segmentation Effect," *IEEE Trans. Magn.,* vol. 48, no. 12, pp. 4831-4841, 2012.
[39] A. Bettayeb, X. Joannot and J. Vannier, "Analytical Calculation of Rotor Magnet Eddy-Current Losses for High Speed IPMSM," *IEEE International Conference on Electric Machine*, 2010, ICEM'10pp. 1-6.
[40] K. Yamazaki and S. Watari, "Loss Analysis of Permanent-Magnet Motor Considering Carrier Harmonics of PWM Inverter Using Combination of 2-D and 3-D Finite-Element Method," *IEEE Trans. Magn.,* vol. 41, no. 5, pp. 1980-1983, 2005.
[41] Y. Kawase, T. Ota and H. Fukunaga, "3-D Eddy Current Analysis in Permanent Magnet of Interior Permanent Magnet Motors," *IEEE Trans. Magn.,* vol. 36, no. 4, pp. 1863-1866, 2000.
[42] K. Yamazaki and A. Abe, "Loss Investigation of Interior Permanent-Magnet Motors Considering Carrier Harmonics and Magnet Eddy Currents," *IEEE Trans. Ind. Appl*., vol. 45, no. 2, pp. 659 - 665, 2009.
[43] X. Wu, R. Wrobel, P.H. Mellor and C. Zhang, "A Computationally Efficient PM Power Loss Derivation for Surface-Mounted Brushless AC PM Machines," *IEEE International Conference on Electric Machine*, 2014, ICEM'14 pp. 17-23.
[44] A. EL-Refaie, "Fractional-Slot Concentrated-Windings Synchronous Permanent Magnet Machines: Opportunities and Challenges," *IEEE Trans. Ind. Electron*., vol. 57, no. 1, pp. 107 - 121, 2010.
[45] Flux2D/3D user's manual, Cedrat, 2014.
[46] S. Ruoho, M. Haavisto, E. Takala, T. Santa-Nokki, M. Paju, "Temperature Dependence of Resistivity of Sintered Rare-Earth Permanent-Magnet Materials ," *IEEE Trans. Magn*.,vol. 46, no. 1, pp. 15-20, January 2010.
[47] R. Krishnan, "Permanent Magnet Synchronous and Brushless DC Motor Drives," Virginia, 2010.

## VIII. BIOGRAPHIES

**Xiaopeng Wu** received B.Eng. degree from Beihang University, Beijing, China in 2006. He is currently working towards an Eng. D degree with the Beijing Institute of Technology and working as a visiting researcher with the Electrical Energy Management Group (EEMG) at the University of Bristol. His research interests include the design and modelling of electrical machines in traction application.

**Rafal Wrobel** received the M.Sc.Eng. degree from the Technical University of Opole, Opole, Poland, in 1998, the Ph.D. degree from the Technical University of Lodz, Lodz, Poland, in 2000 and the Habilitation degree from the Technical University of Opole, Opole, Poland, in 2013. (2000-2002), he was an Assistant Professor with the Technical University of Opole. (2002-2011) he was a Research Fellow with the Electrical Energy Management Group (EEMG) at the University of Bristol, Bristol, U.K. Since 2011, he has been a Senior Research Fellow with the EEMG, and his research interests include multi-physics and multi-disciplinary design-analysis of electrical machines and wound passive components.

**Phil H. Mellor** received the B.Eng. and Ph.D.degrees in electrical engineering from the Department of Electrical Engineering, Liverpool University, Liverpool, U.K., in 1978 and 1981, respectively.
He is currently a Professor of electrical engineering with the Department of Electrical and Electronic Engineering, University of Bristol, Bristol, U.K. Prior to this, he held academic posts at The University of Liverpool, Liverpool, U.K. (1986 to 1990) and The University of Sheffield, Sheffield, U.K. (1990 to 2000). His research activities include high-efficiency electric drives, and actuation and generation systems for application in more electric aircraft and hybrid-electric vehicles.

**Chengning Zhang** received the M.E. degree from control theory and control engineering and the Ph.D. degree in vehicle engineering from the Beijing Institute of Technology, Beijing, China, in 1989 and 2001, respectively. He is currently a Professor and Vice Director of the National Engineering Laboratory for Electric Vehicles, Beijing Institute of Technology. His research interests include electric vehicles, vehicular electric motor drive systems, battery management systems, and chargers.